Solid State Ionics 247–248 (2013) 8–14

Contents lists available at SciVerse ScienceDirect

Solid State Ionics

journal homepage: www.elsevier.com/locate/ssi

First-principles investigation of Li ion diffusion in Li_2FeSiO_4

Rafael B. Araujo [a,b,c,*], Ralph H. Scheicher [b], J.S. de Almeida [a], A. Ferreira da Silva [a], Rajeev Ahuja [b,c]

[a] Universidade Federal da Bahia, Instituto de Física, Campus Ondina 40210 340 Salvador, Bahia, Brazil
[b] Condensed Matter Theory Group, Department of Physics and Astronomy, Uppsala University, PO Box 516, SE-751 20 Uppsala, Sweden
[c] Applied Materials Physics, Department of Materials and Engineering, Royal Institute of Technology (KTH), SE-100 44 Stockholm, Sweden

ARTICLE INFO

Article history:
Received 21 January 2013
Received in revised form 19 May 2013
Accepted 31 May 2013
Available online 25 June 2013

Keywords:
Lithium diffusion
Batteries
DFT

ABSTRACT

We have studied the Li-ion migration and the electrochemical performance of Li_2FeSiO_4 in the monoclinic crystal structure with $P2_1$ symmetry and the related delithiated system $LiFeSiO_4$. For this purpose, the framework of the density functional theory within the generalized gradient approximation in conjunction with the climbing image nudged elastic band method was used. Addition of the Hubbard term was also considered in the Kohn–Sham Hamiltonian to better model the *d* electrons of the metal ions in this material. The calculated activation energies for Li ion migration are found to decrease by around 20% with the Hubbard term inclusion in the chosen diffusion pathways of Li_2FeSiO_4. Regarding the delithiated structure, the activation energies were found to be sensitive to the Hubbard term addition, however no general behavior such as in the lithiated structure was found. Furthermore, the diffusion coefficients were calculated considering temperatures of 300 K, 500 K, and 700 K.

1. Introduction

The development of new materials for application in cathodes of Li-ion batteries is an intensive area of research. This is due to the wide range of applicability of these batteries, such as in hybrid electric vehicles or electronic devices. Much of the battery cost is associated with the selection of the cathode material. Li_2FeSiO_4 was synthesized and characterized by Nytén *et al.* [1] as an alternative cathode material with low cost and good performance. Numerous experiments [1–12] and theoretical calculations [13–18] have been carried out on this material, showing advantages such as environmental benignity, high cycle stability, and a theoretical capacity as high as 166 mAh g^{-1}. Regarding the crystal structure, Nytén *et al.* [1] proposed an orthorhombic lattice with $Pmn2_1$ space group. However, a report on Li_2FeSiO_4 by Nishimura *et al.* [19] suggested a different structure with a monoclinic type and a $P2_1$ symmetry. The main difference between the two structures is that the orthorhombic ($Pmn2_1$) structure has the FeO_4–SiO_4 tetrahedra all aligned in the same direction [1] whereas in the monoclinic ($P2_1$) structure the FeO_4–SiO_4 tetrahedra alternately point in opposite directions [19].

The structural and electronic properties of monoclinic Li_2FeSiO_4 were not investigated extensively. In Ref. [20] a study of the stability, electronic properties, and electrochemical performance of the $P2_1$ structure was presented. The diffusion mechanism was investigated in Ref. [21], indicating a two-dimensional diffusion of the ions in Li_2FeSiO_4. The present work aims to investigate the migration mechanisms of Li ions in monoclinic Li_2FeSiO_4, as well as the electrochemical performance of this material considering the influence of the Hubbard term addition to the Kohn–Sham Hamiltonian in the lithium diffusion process. The framework of density functional theory (DFT) was used together with the climbing image nudged elastic band method (cNEB) to gain insights about the lithium migration pathways as well as the diffusion barriers.

This paper will be organized as follows. In Section 2, we present the theoretical background and the computational details along with the computational parameters used in this work. The structural stability of Li_2FeSiO_4 as well as that of $LiFeSiO_4$ was studied in detail in Section 3. The results of the open circuit voltage (OCV) calculations and the influence of the Hubbard term inclusion in the Kohn–Sham Hamiltonian as well as the influence of the magnetic state on it are presented in Section 4. In Sections 5 and 6 we present the lithium migration results together with the diffusion coefficients. Finally, we conclude with a brief summary of the reported results provided by our *ab initio* calculations in Section 7.

2. Computational details

In order to reach a better understanding of the electronic and structural properties of Li_2FeSiO_4 and the delithiated system $LiFeSiO_4$, we performed DFT-based *ab initio* calculations based on the projector augmented wave (PAW) method as implemented in the Vienna *Ab initio* Simulation Package (VASP) [22,23]. The exchange and correlation

* Corresponding author at: Universidade Federal da Bahia, Instituto de Física, Salvador, Bahia, Brazil.
E-mail addresses: rafaelbna@gmail.com (R.B. Araujo), rajeev.ahuja@fysik.uu.se (R. Ahuja).

0167-2738/$ – see front matter © 2013 Elsevier B.V. All rights reserved.
http://dx.doi.org/10.1016/j.ssi.2013.05.020

terms are treated within the spin-polarized generalized gradient approximation (GGA) in the Perdew and Wang parameterization (PW91) [24].

To take into account the localization of the *d* electrons in the transition metal ions in this material, we employed the GGA + U approach of Dudarev *et al.* [25]. At this level, the Hubbard repulsion term, *U*, and the exchange term, *J*, do not enter separately in the Hamiltonian. In this case, only a single effective parameter $U_{eff} = U\text{-}J$ is taken into account (we will refer to U_{eff} in the following simply as *U*). The *U* value is selected to match the calculated band gap with the experimental value. It is well-known that DFT fails to reproduce band gaps of transition metal oxides. Therefore, we have used $U =$ 5 eV, which was shown by previous investigations [14,18,20,21] to be a suitable value to reproduce the related features such as the open circuit voltage. The energy cut-off for the wave function expansion was set to 700 eV. Integrals were calculated over the Brillouin zone by the Gaussian smearing method with *k*-points based on a $4 \times 6 \times 4$ Monkhorst-Pack grid [26]. In the first part of this research, we performed calculations in the antiferromagnetic (AFM), ferromagnetic (FM), and paramagnetic (PM) configurations. For the second part, all the calculations were carried out in the AFM configuration since it was found by us to be the most stable magnetic configuration considering the GGA + U scheme.

The Li^+ diffusion in the Li_2FeSiO_4 and $LiFeSiO_4$ crystal structures were investigated with the climbing image nudged elastic band method [27,28] in a $2a \times 2b \times c$ supercell containing 16 formula units corresponding to 128 atoms (lithiated system) and 112 atoms (delithiated systems), respectively. The large supercell dimensions separate the atoms from their periodic image, ensuring an accurate answer to the activation barrier in the diluted limit. A lithium vacancy was created in the supercell of the Li_2FeSiO_4, while an extra lithium atom was added to the supercell of the $LiFeSiO_4$. By adding or removing a Li atom (Li^+ and e^-) in the delithiated and lithiated systems we are properly modeling the redox reaction that occurs in the cathode during the charge and discharge process of the battery. It should be noticed that the oxide lattice displays a strong oxidative environment, and, for instance, considering the charge process, as the reducing equivalent pair (Li^+ and e^-) is removed the Fe ion around the vacancy undergoes an oxidation state change from Fe^{2+} to Fe^{3+}, and the Li atoms stay in the charge state 1+, in order to keep the oxygen charge state 2−. Therefore, the migrating species in the lattice are the Li^+ ions. Having adopted this procedure, we can now have insights about the lithium ion diffusion pathways in both structures (considering charged lithium battery, $LiFeSiO_4$, and discharged lithium battery, Li_2FeSiO_4). The geometries of the created supercells were relaxed taking into account the defects. It was noticed that the lattice parameters *a*, *b*, and *c* of the relaxed supercell with defects change only 0.18% from their unrelaxed values for the supercell without defects. Therefore, even considering that we performed defect calculations, we decided to keep the full relaxation of the supercell. Furthermore, the atoms placed further away from the defect site did not move much from their original positions in both cases due to the big size of the supercell. These calculations were performed using a 400 eV cutoff and only one *k* point (Γ point) due to the large size of the supercell. Geometry optimizations were considered converged when the forces on each atom were less than 5 meV/Å.

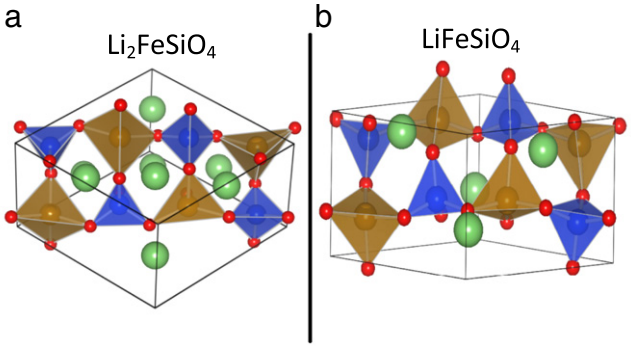

Fig. 1. Crystal structures of (a) Li_2FeSiO_4 and (b) $LiFeSiO_4$. Here, red spheres represent oxygen, blue spheres (inside semi-transparent blue tetrahedra) represent silicon, brown spheres (inside semi-transparent brown tetrahedra) represent iron, while green spheres represent lithium ions.

Table 1
Results of the lattice parameters optimization in Li_2FeSiO_4 and the associated relative total energy. The corresponding magnetic ground state has been assigned zero energy: Ferromagnetic for GGA and antiferromagnetic for GGA + U.

	a (Å)	*b* (Å)	*c* (Å)	α(°)	β(°)	γ(°)	*V* (Å^3)	Δ*E* (eV)
AFM-GGA	8.26	5.09	8.25	90	99,04	90	343.38	0.04
FM-GGA	8.25	5.12	8.25	90	99.25	90	344.52	0.00
PM-GGA	8.22	5.00	8.21	90	101.42	90	331.00	1.94
AFM-GGA + U	8.31	5.08	8.28	90	99.07	90	345.99	0.00
FM-GGA + U	8.32	5.09	8.28	90	99.27	90	346.15	0.04
PM-GGA + U	8.35	4.87	8.45	90	102.33	90	331.61	2.83
EXP.	8.22	5.02	8.23	90	99.20	90	335.74	–

To determine the minimum energy path (MEP) through the cNEB method, six replicas of the system were created, in which the diffusing Li atom was moved in equidistant steps to positions between the initial and final states for the path obtained from linear interpolation. Ionic position optimizations of the replicas were allowed in order to minimize the total energy. Furthermore, each image is connected with its neighbor images through a spring and the highest energy replica is driven up to the saddle point [27]. Calculated activation energies converged within 0.02 eV.

3. Crystal structure

The crystal structure for Li_2FeSiO_4 was taken from Ref. [19]. The experiment revealed a monoclinic structure with $P2_1$ point symmetry, with lattice parameters $a = 8.29$ Å, $b = 5.02$ Å and $c = 8.23$ Å and $\alpha = \gamma = 90^\circ$ and $\beta = 99.2^\circ$. Fig. 1a shows this crystal structure. It consists of a lattice built up from infinite conjugated layers of composite $SiFeO_4$ linked through the LiO_4 tetrahedra, with each Li, Fe, Si located in the center of the tetrahedra formed by four oxygen atoms. Furthermore, the Li^+ ions are occupying tetrahedra sites between the FeO_4–SiO_4 where the tetrahedra alternately point in opposite directions. The atomic fractional coordinates and the crystallographic cell shape were relaxed for different magnetic states. Table 1 presents a summary of the optimized results.

To analyze the magnetic configuration in this crystal lattice we have calculated the total energy per formula unit in different magnetic configurations and considered the ground state energy as the reference (zero energy). In the GGA approximation, the ground state appears to be a FM configuration; however, at the GGA + U level, it is revealed that the AFM configuration possesses the lowest energy. The energy difference between the AFM and FM, in both cases, appears to be quite small (37 meV/f.u.).

Table 2
Results of the lattice parameters optimization in $LiFeSiO_4$ and the associated relative total energy. The corresponding magnetic ground state has been assigned zero energy: Ferromagnetic for GGA and antiferromagnetic for GGA + U.

	a (Å)	*b* (Å)	*c* (Å)	α(°)	β(°)	γ(°)	*V* (Å^3)	Δ*E* (eV)
AFM-GGA	8.25	5.14	8.26	90.00	93.49	90.00	350.39	0.02
FM-GGA	8.26	5.15	8.27	90.00	93.49	90.00	351.63	0.00
PM-GGA	8.23	4.97	8.22	89.99	96.20	89.98	334.96	1.91
AFM-GGA + U	8.25	5.14	8.26	90.00	93.51	89.99	350.05	0.00
FM-GGA + U	8.25	5.14	8.27	90.00	93.50	89.99	350.43	0.01
PM-GGA + U	8.21	4.98	8.23	90.00	94.46	90.00	336.77	3.38

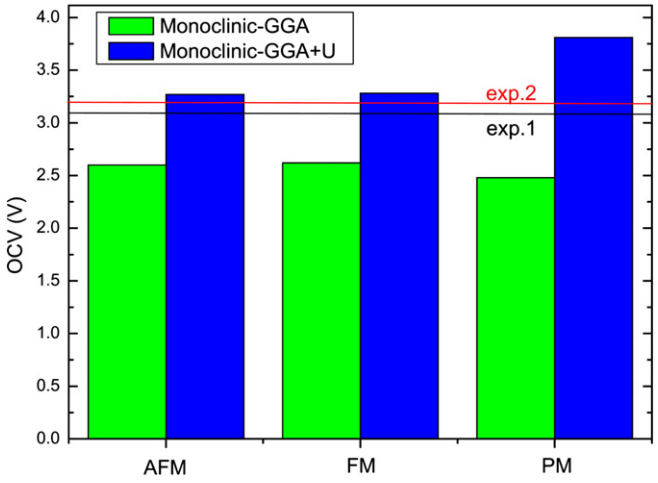

Fig. 2. Average voltages for Li extractions from Li_2FeSiO_4 calculated using GGA (green) and GGA + U (blue) for the different magnetic states. For comparison, experimentally measured voltages are also presented as red [1,3] and black [4] lines.

Comparing the lattice parameters, one observes a good agreement with the experimental data and a small difference between the calculations using GGA and GGA + U.

To find the crystal structure of the $LiFeSiO_4$ system we started from the optimized Li_2FeSiO_4 and chose three different patterns to select half of the Li atoms for removal. In this sense, a new optimization of the crystallographic cell parameters (the cell shape as well as the lattice constants) and the atomic fractional coordinates were allowed to change until the forces on all atoms were less than 0.01 eV/Å. Fig. 1b shows the configuration which possesses the lowest total energy. Table 2 lists the resulting structural and energetic properties of the relaxed delithiated system. The obtained structure cannot be guaranteed to be the ground state since it was only relaxed from the initial monoclinic cell. One can notice a unit cell expansion compared to Li_2FeSiO_4 due to the additional Li^+ ions that hold the lattice tighter together in the case of the fully lithiated system, and therefore leading to a smaller volume. The structure reveals again a FM configuration in the GGA approach and an AFM configuration for the GGA + U approach, although with even smaller energy difference between the ground state and the next highest state compared to Li_2FeSiO_4 in both cases (GGA and GGA + U).

4. Average deintercalation voltages

To test whether the determined structures realistically represent the systems in question, we calculated the open circuit voltage (OCV) and compared it with its respective experimental value. For that we followed the well-established methods [29,30] in which the OCV is calculated by $\overline{V} = -\Delta G_r/\Delta x$ where Δx refers to the number of lithium transferred, and ΔG_r is the Gibbs free energy difference between two intercalation limits. The relative volume change when one removes the lithium atoms from the Li_2FeSiO_4 structure is of the order of 1%. At atmospheric pressure that expansion will yield a Gibbs free energy variation lower than 10^{-7} eV. At ambient conditions, the variation of entropy produces change in energy of about 10^{-3} eV. Therefore, the main contribution to the Gibbs free energy change will come from the variation of the internal energy of our system (around 3 eV) allowing us to neglect the volume and entropy effects in the OCV calculation. Thus, the OCV can be written as:

$$OCV \approx \frac{E(LiFeSiO_4) + xE(Li) - E(Li_{1+x}FeSiO_4)}{x}. \quad (1)$$

The fully lithiated system corresponds to $x = 1$.

Therefore, to calculate the OCV, the total energy of the lithiated and delithiated systems was determined in the GGA and GGA + U approaches. The total energy of metallic Li represented in Eq. (1) as $E(Li)$ was calculated in the *bcc* structure, which is the structural phase of the Li anode.

Fig. 2 presents the calculated average voltages for the Fe^{2+}/Fe^{3+} reactions in the different magnetic configurations as well as with and without the Hubbard term. It is observed that the potential calculated at the GGA level is always lower than the experimentally measured values. The results found for GGA + U are slightly higher than experiment, but in much better agreement than the GGA approach. Considering the magnetic states, the OCV for both AFM and FM agree almost equally well with the experimental results. This result confirms the importance of taking into account the Hubbard term when calculating the average intercalation potential in this material.

5. Lithium migration results

In order to have a better understanding of the lithium diffusion in the crystal structure of the lithiated and delithiated systems we constructed a $2a \times 2b \times c$ supercell and created a vacancy in the Li_2FeSiO_4 supercell, while a new atom was incorporated in the $LiFeSiO_4$ supercell crystal structure. After this step we performed a new optimization at the GGA and GGA + U levels in both systems. The results of the optimization process in the lithiated system leads to lattice parameters of $a = 8.1725$ Å, $b = 5.0132$ Å and $c = 8.16502$ Å in the GGA approach and for the GGA + U scheme they become $a = 8.2147$ Å, $b = 4.9684$ Å and $c = 8.2118$ Å. One notices that there exists a small difference when comparing values of the lattice parameters between the two different schemes. The lattice parameters of the half-lithiated system after the optimization are $a = 8.0864$ Å, $b = 4.9826$ Å and $c = 8.1056$ Å, and $a = 8.1092$ Å, $b = 4.9809$ Å and $c = 8.1122$ Å for the GGA and GGA + U schemes respectively. In the half-lithiated system, the differences for a, b and c are quite small. All calculations for the lithium diffusion were carried out in the AFM configuration since based on our previously described results, we found that this appears to be the preferred magnetic configuration at low temperatures. The results for the supercells optimization show that the smallest distance between two periodic replicas is about 8 Å, which should ensure that the interaction between periodically repeated entities will presumably be small enough to be neglected.

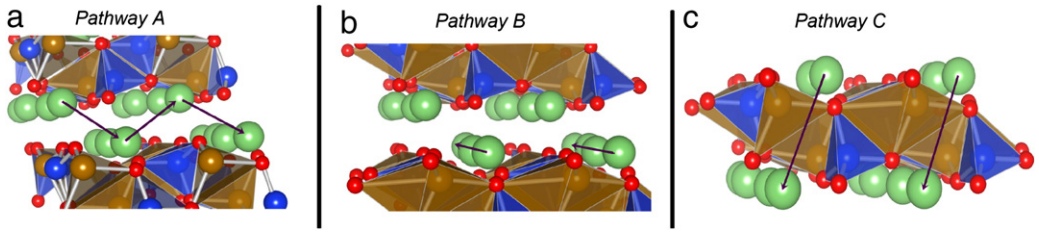

Fig. 3. Three possible pathways for Li ion migration in monoclinic Li_2FeSiO_4 .

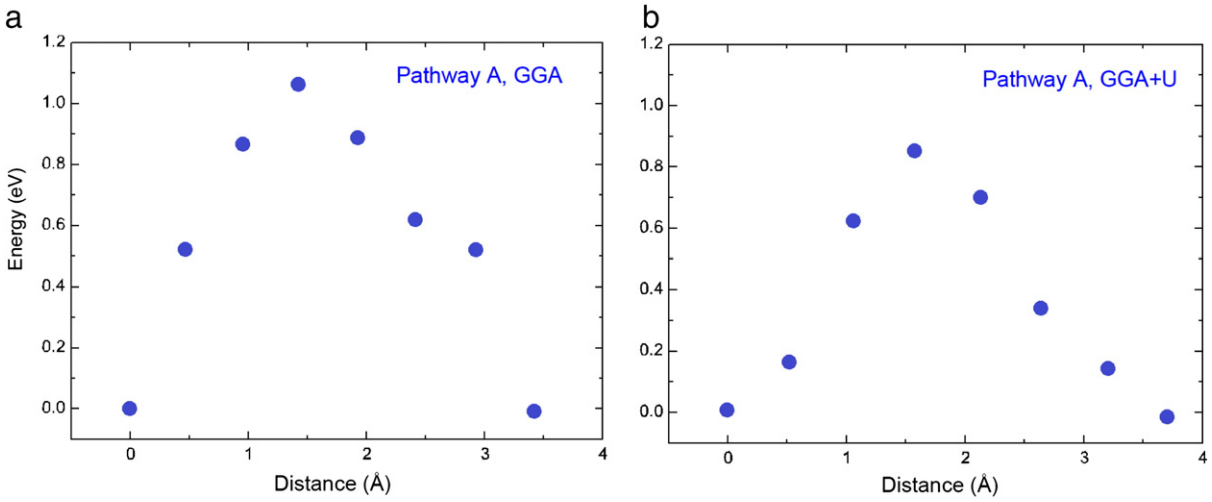

Fig. 4. Lithium ion migration in monoclinic Li_2FeSiO_4 for pathway A as obtained from cNEB method. Blue symbols represent calculated data points. Here, (a) represents calculations carried out in the GGA approximation while (b) represents calculations performed at the GGA + U level.

5.1. Lithiated system (Li_2FeSiO_4)

When analyzing the crystal structure for the lithiated and the delithiated systems, we observe three potential paths for Li^+ hopping as shown in Fig. 3. Pathway A is characterized by a zigzag trajectory with the Li ions moving between the Si–Fe–O layers. The hopping distance in this case is 3.5 Å. Pathway B is characterized by a linear motion of the Li ions between the layers. The hopping distance here amounts to 3.9 Å between the neighboring equilibrium sites. For the pathway C, Li migration occurs through the Fe–Si–O layers with a hopping distance of 4.7 Å. The cNEB calculations reveal that pathway A possesses the lowest activations energy. Fig. 4 shows the results for the activation energy in pathway A. We find a 1.06 eV barrier in the GGA approach, while for the GGA + U scheme this value decreases to 0.84 eV. The use of the GGA + U scheme leads to a change of the electronic structure localizing electrons. It suggests that the resultant Coulombic interaction felt by the Li^+ ion at the saddle point in the GGA + U method leads to lower activation energy. The activation barrier in the GGA + U approach for pathway A matches quite well with that presented in Ref. [21] which is 0.83 eV. Pathway B possesses an activation energy of 1.21 eV in the GGA approach and 0.95 eV for the GGA + U scheme. Finally, the activation energy calculated for pathway C is 1.8 eV in the GGA and 1.79 eV in the GGA + U. Therefore, it can be regarded as unlikely that the lithium diffusion would follow this pathway since it entails a high activation energy coming from the large electrostatic repulsion created by the Fe–Si–O layers. Table 3 shows the distance between the closest atoms and the lithium ion at the transition state in pathway A and pathway B. One can note that these distances in the GGA and GGA + U approaches are quite different resulting in different electrostatic repulsion felt by the Li ion and thus reflected in the magnitude of the activation barrier. It is observed that the Li–Fe distance tends to increase when one changes from GGA to GGA + U schemes for both pathways. This is a result of the higher Coulombic repulsion between the lithium ion and the localized hole in GGA + U approach. It is also responsible for the reduction of the Li–Si and Li–O bonds noticed in Table 3 when we change the exchange and correlation functional. Finally, the activation energy calculated for pathway C is 1.8 eV in the GGA and 1.79 eV in the GGA + U. Therefore, it can be regarded as unlikely that the lithium diffusion would follow this pathway since it entails a high activation energy coming from the large electrostatic repulsion created by the Fe–Si–O layers. Therefore, the pathway with the highest likelihood for lithium migration is pathway A and, as the energy difference between pathways A and B is with 0.1 eV not too large, it can be assumed that path B might contribute as well to the lithium diffusion. Table 4 presents a summary of the activation energy for the lithiated system.

The migration pathways and diffusion barriers for Li-ions in the Li_2FeSiO_4 $Pmn2_1$ orthorhombic structure were investigated in Ref. [31]. The framework of the density functional theory was used in the GGA approach to treat the exchange and correlation terms. They reported an activation barrier of 0.83 eV to the most probable migration path regarding the lithiated state. Comparing our results to the activation energy in the most probable path (1.06 eV in the GGA approach) with the presented one in Ref. [31], it is possible to notice a difference of around 20%. It raises the idea that the orthorhombic structure could actually show greater Li^+ diffusion into its atomic structure. However, to get a final answer for this discussion, the DFT calculations in Ref. [31] should have been done considering the Hubbard term to properly model the *d* electrons interaction. Our results of the calculated activation energies in Li_2FeSi_4 showed that the activation energy decreased from 1.06 eV down to 0.84 eV when we took into account the Hubbard term. Meanwhile, it is not clear that the activation energy will follow the same behavior in the orthorhombic structure considering the Hubbard term. For example, theoretical studies were carried out considering the crystal structure of the $LiFePO_4$ in order to understand lithium migration mechanisms [32].

Table 3
Distances between the Li ion in the transition state and the nearest neighbor atoms in the pathway A and pathway B considering Li_2FeSiO_4 crystal structure.

		Li–O (Å)	Li–Si (Å)	Li–Fe (Å)
Pathway A	GGA	1.79	2.66	2.65
	GGA + U	1.76	2.52	2.70
Pathway B	GGA	1.76	2.57	2.74
	GGA + U	1.75	2.50	2.87

Table 4
Results for hopping distance and activation barrier calculations (ΔE) in monoclinic Li_2FeSiO_4 with both GGA and GGA + U.

	Functional	Distance (Å)	ΔE (eV)
Pathway A	GGA	3.5	1.06
	GGA + U	3.7	0.84
Pathway B	GGA	3.9	1.21
	GGA + U	3.9	0.95
Pathway C	GGA	4.7	1.80
	GGA + U	4.8	1.79

Table 5
Results for hopping distance and activation barrier calculations (ΔE) in monoclinic $LiFeSiO_4$ with both GGA and GGA + U.

	Functional	Distance (Å)	ΔE (eV)
Pathway A	GGA	3.00	0.40
	GGA + U	2.76	0.56
Pathway B	GGA	4.00	0.42
	GGA + U	3.72	0.36
Pathway C	GGA	4.70	1.62
	GGA + U	5.05	1.76

They have reported no difference for the activation energies values when the Hubbard term is taken into account or not. They also showed that lower or high barriers can be found for this material if electrons localized with DFT + U are able to move in a reaction.

5.2. Delithiated system ($LiFeSiO_4$)

The calculations for the delithiated system followed the same procedure as applied in the previous case for the lithiated system. Pathway A entails an activation barrier of about 0.40 eV and 0.56 eV for the GGA and GGA + U approaches, respectively. Unlike for the lithiated system, we observe here an increase in the activation barrier when going from GGA to the GGA + U method in pathways A and C, while pathway B exhibits a decrease in the activation energy as shown in Table 5 and discussed further below. The difference of the total energy revealed in Fig. 5 for the initial and final states is a consequence of the different symmetry of these sites. Comparing the activation energy of pathway A in the lithiated and delithiated systems, a reduction of the value can be noted independently of the addition of the Hubbard term. The value of the supercell volume in $LiFeSiO_4$ is greater than in the lithiated system, which leads to a more open crystal structure allowing an easier motion of the Li ions. Therefore, the Li ions feel a lower electrostatic repulsion coming from the neighboring atoms in the delithiated system, resulting in a smaller activation energy. Table 5 shows a summary of the activation barriers in the delithiated system.

Pathway B exhibits an activation energy of 0.42 eV and 0.36 eV in the GGA and GGA + U approach, respectively. One can observe in Table 5 that the reduction of the activation barrier value associated with the Hubbard term leads to a change in the more probable pathway. For the GGA calculation, pathways A and B exhibit almost the same value for the activation energy revealing a difference of 0.02 eV, therefore, at this level of approximation, both pathways would likely contribute to the lithium motion. Considering the GGA + U scheme this difference increases however to 0.2 eV and reverses its order. As in the case of the lithiated system, pathway C reveals a rather high activation energy, which will inhibit diffusion through this path. Comparing our computational results of the activation energy with those presented in Ref. [21] for $LiFeSiO_4$, one notices a difference of around 0.4 eV for the lower activation energy pathway. This fact is a result of differently chosen paths for the Li migration. Here, we have decided to investigate pathways closer to the chosen paths in the Li_2FeSiO_4 crystal structure. These differences between the paths to the Ref. [21] and ours are confirmed with the revealed hopping distance value. They got values until 11 Å for this quantity while we have an average value of around 3.5 Å. Another point is the way we model the ion migration in the half-lithiated system. We have introduced a new Li atoms (Li^+ more e^-) into the $LiFeSiO_4$ crystal structure with the main idea to correctly describe the battery discharge process. However, even with these differences, both works agree with the fact that the lithium diffusion in the half-lithiated system would not occur preferentially in a zigzag trajectory between adjacent minimum energy sites if one takes into account the Hubbard term.

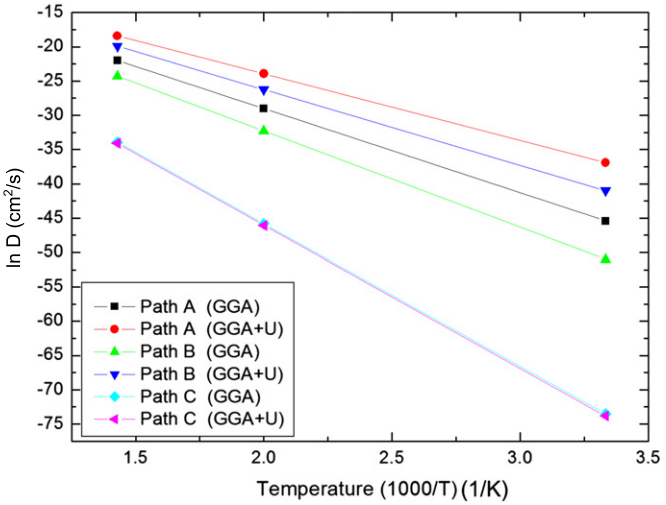

Fig. 6. Natural logarithm of the diffusion coefficient against 1/T for the lithiated system in different pathways using GGA and GGA + U functionals.

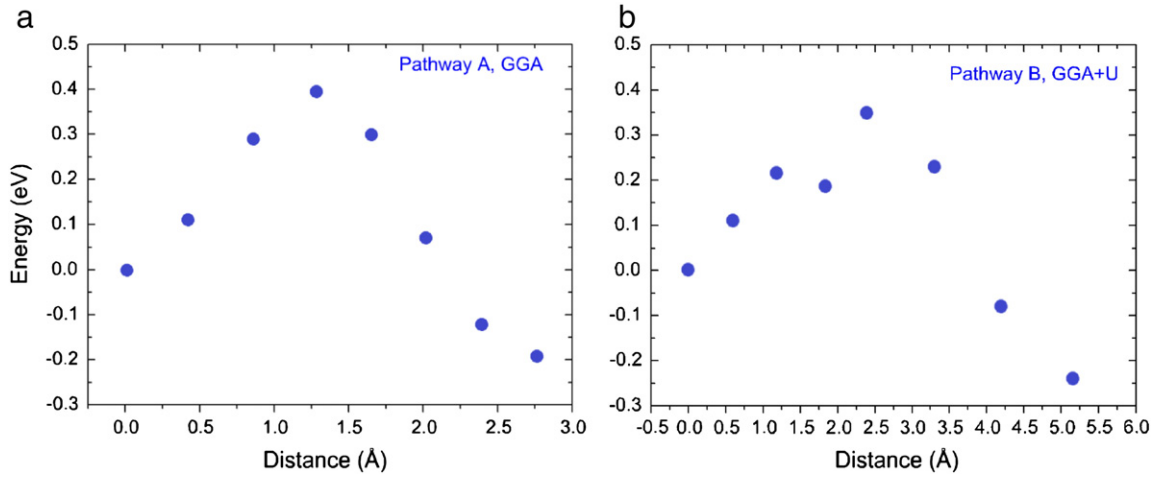

Fig. 5. Lithium ion migration in monoclinic $LiFeSiO_4$. Blue symbols represent the calculated data. Here, (a) represents calculations carried out in the GGA approximation to the pathway A while (b) represents calculations performed at the GGA + U level in the pathway B.

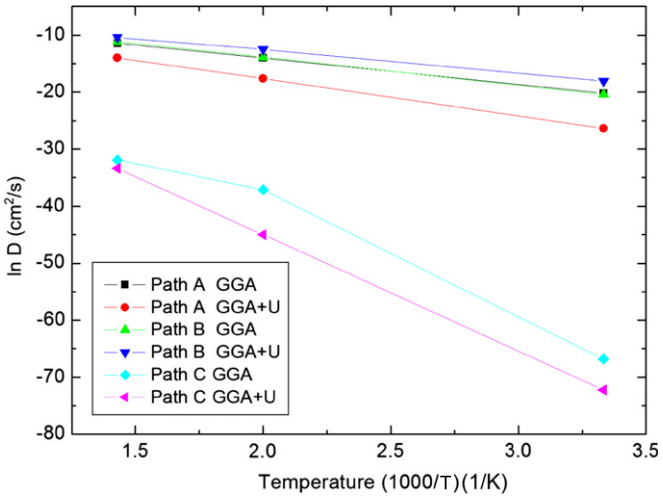

Fig. 7. Natural logarithm of the diffusion coefficient against 1/T for the delithiated system in different pathways using GGA and GGA + U functionals.

6. Diffusion coefficient

The lithium diffusion coefficient can be calculated as $D = d^2\Gamma$, where d is the hopping distance and Γ is the hopping rate being defined in the transition state theory [33] as $\Gamma = \nu_0 exp(-E_a/k_BT)$. In this case, E_a is the activation energy, k_B is the Boltzmann constant, T is the temperature, and ν_0 is the attempt frequency. Therefore the diffusion constant D can be written as:

$$D = d^2\nu_0 exp\left(-\frac{E_a}{k_BT}\right). \quad (2)$$

All calculations for the diffusion coefficient were performed considering ν_0 about 10^{13} Hz, which is in the range of the phonon frequencies and consistent with typical values for the attempt frequency [34]. For the temperature we considered 300 K, 500 K, and 700 K. Fig. 6 summarizes all diffusion coefficients for the lithiated system. Since we have plotted the natural logarithm of the diffusion coefficient against 1/T, we can see that the activation barrier is proportional to the slope of each straight line.

Analyzing the results for Li_2FeSiO_4, it is possible to notice a difference in the diffusion coefficient when one takes into account the Hubbard term. These differences come from the fact that the usage of this scheme leads to a change in the crystal structure of the system. Pathway A reveals the highest value to the diffusion coefficient in both approaches for the exchange and correlation term. This indicates a zigzag lithium migration with the diffusion to take place between the shortest linear Li sites. Pathway B also contributes to the lithium migration, however it exhibits a high activation barrier. The diffusion coefficient in the Li_2FeSiO_4 crystal structure is significantly lower than what was found for other common cathode materials at room temperature. For example, for the commercially used Li_xCoO_2 the diffusion coefficient has been found to be within the range of 10^{-13} to 10^{-7} cm^2/s at room temperature [34].

Fig. 7 summarizes the obtained results for the diffusion coefficient in the delithiated crystal structure. The GGA calculations present a diffusion coefficient rather similar for pathway A and pathway B. However, a change in this behavior is noted when the Hubbard term is added to the Kohn–Sham Hamiltonian. In this case, pathway A reveals a substantial reduction of the diffusion coefficient while pathway B shows a slight increase in value. Therefore, considering the GGA approach, the lithium diffusion appears to be two-dimensional with the Li ions traveling through pathway A and B, while with the addition of the Hubbard term the diffusion becomes one-dimensional going through pathway B. Comparing the results for the lithiated and delithiated systems we observe an increase in the diffusion coefficient for the delithiated system.

7. Conclusions

In this paper, we studied different migration paths for lithium in the Li_2FeSiO_4 crystal structure. We identified those which yield the lowest barrier and are thus most likely to contribute to the Li diffusion. Our results reveal that the most probable migration path in the lithiated system is the one in which Li ions follow a zigzag way between the Fe–Si–O layers (pathway A). However, the activation barrier calculated for pathway B is quite close to that for pathway A, thus making it possible to consider that this path can also contribute to the Li ion migration leading to a two-dimensional diffusion. The addition of the Hubbard term is affecting the activation barrier but it does not change the character of the most probable diffusion path.

Calculations for the delithiated system reveal two different situations: when one is not considering the Hubbard term, the Li migration is two-dimensional; however within the GGA + U scheme the diffusion becomes one-dimensional. The reason for this is that the inclusion of the Hubbard term leads to the activation energy difference between pathway A and B to become greater, making pathway B the most probable one.

Finally, when comparing the diffusion coefficient in Li_2FeSiO_4 at room temperature, ranging from 10^{-20} cm^2/s up to 10^{-17} cm^2/s, with the diffusion coefficient in currently used materials typically ranging from 10^{-13} cm^2/s to 10^{-7} cm^2/s [34], it is seen clearly that Li_2FeSiO_4 can at the moment not provide better kinetics than the state-of-the-art materials. More work is thus needed to improve ion diffusion in this material.

Acknowledgements

We are thankful to the financial support from the Brazilian agencies CNPq, CAPES and FAPESB (Bahia) and the Swedish funding agencies VR, FORMAS. Resources of the Swedish National Infrastructure for Computing (SNIC), National Supercomputer Center (NSC) and the Uppsala Multidisciplinary Center for Advanced Computational Science (UPPMAX) are also gratefully acknowledged.

References

[1] A. Nytén, A. Abouimrane, M. Armand, T. Gustafsson, J.O. Thomas, Electrochem. Commun. 7 (2005) 156.
[2] A. Nytén, S. Kamali, L. Häggström, T. Gustafsson, T.O. John, J. Mater. Chem. 16 (2006) 2266.
[3] R. Dominko, M. Bele, M. Gaberscek, A. Meden, M. Remskar, J. Jamnik, J. Electrochem. Commun. 8 (2006) 217.
[4] Z.L. Gong, Y.X. Li, Y. Yang, Electrochem. Solid State Lett. 9 (2006) A542.
[5] K. Zaghib, A.A. Salah, N. Ravet, A. Mauger, F. Gendron, Julien, J. Power. Sources 160 (2006) 1381.
[6] A. Nytén, M. Stjerndahl, R. Håkan, S. Hans, A. Michel, G. Torbjörn, E. Kristina, O.T. John, J. Mater. Chem. 16 (2006) 3483.
[7] R. Dominko, M. Bele, A. Kokalj, M. Gaberscek, J. Jamnik, J. Power. Sources 174 (2007) 457.
[8] Z.L. Gong, Y.X. Li, Y. Yang, J. Power. Sources 174 (2007) 524.
[9] Y.X. Li, Z.L. Gong, Y. Yang, J. Power. Sources 174 (2007) 528.
[10] V.V. Politaev, A.A. Petrenko, V.B. Nalbandyan, B.S. Medvedev, E.S. Shvetsova, J. Solid State Chem. 180 (2007) 1045.
[11] R. Dominko, D.E. Conte, D. Hanzel, M. Gaberscek, J. Jamnik, J. Power. Sources 178 (2008) 842.
[12] R. Dominko, J. Power. Sources 184 (2008) 462.
[13] P. Larsson, R. Ahuja, A. Nytén, T.O. Thomas, Electrochem. Commun. 8 (2006) 797.
[14] M.E. Arroyo-de Dompablo, M. Armand, J.M. Tarascon, U. Amador, Electrochem. Commun. 8 (2006) 1292.
[15] S.Q. Wu, J.H. Zhang, Z.Z. Zhu, Y. Yang, Curr. Appl. Phys. 7 (2007) 611.
[16] M.E. Arroyo-de Dompablo, R. Dominko, G.M. Gallardo-Amores, L. Dupont, G. Mali, H. Ehrenberg, J. Jamnik, E. Morán, Chem. Mater. 20 (2008) 5574.
[17] M.E. Arroyo-de Dompablo, J.M. Gallardo-Amores, J. García- Martínez, E. Morán, J.M. Tarascon, M. Armand, Solid State Ionics 179 (2008) 1758.
[18] S.Q. Wu, Z.Z. Zhu, Y. Yang, Z.F. Hou, Comput. Mater. Sci. 44 (2009) 1243.
[19] S. Nishimura, S. Hayase, R. Kanno, M. Yashima, N. Nakayama, A. Yamada, J. Am. Chem. Soc. 130 (2008) 13212.

[20] Z. Guohua, L. Yanling, Y. Peng, L. Zhuang, X. Maohai, L. Haiqing, J. Phys. Chem. C 114 (2010) 3693.
[21] S. Dawei, A. Hyojun, W. Guoxiu, Appl. Phys. Lett. 99 (2011) 141909.
[22] G. Kresse, J. Hafner, Phys. Rev. B 47 (1993) 558.
[23] G. Kresse, J. Hafner, Phys. Rev. B 54 (1996) 11169.
[24] J.P. Perdew, J.A. Chevary, S.H. Vosko, K.A. Jackson, M.R. Pederson, D.J. Singh, C. Fiolhais, Phys. Rev. B 46 (1992) 6671.
[25] S.L. Dudarev, G.A. Botton, S.Y. Savrasov, C.J. Humphreys, A.P. Sutton, Phys. Rev. B 57 (1998) 1505.
[26] P.E. Blöchl, O. Jepsen, O.K. Andersen, Phys. Rev. B 49 (1994) 16223.
[27] H. Jonsson, G. Mills, K.W. Jacobsen, in: B.J. Berne, G. Ciccotti, D.F. Coker (Eds.), Classical and Quantum Dynamics in Condensed Phased Simulations, World Scientific, River Edge, NJ, 1998, p. 385.
[28] G. Henkelman, H.J. Jonsson, Chem. Phys. 113 (2000) 9978.
[29] I.A. Courtney, J.S. Tse, O. Mao, J. Hafner, J.R. Dahn, Phys. Rev. B 58 (1998) 15583.
[30] M.K. Aydinol, A.F. Kohan, G. Ceder, K. Cho, J. Joannopoulos, Phys. Rev. B 56 (1997) 1354.
[31] A. Liivat, J.O. Thomas, Solid State Ionics 192 (2007) 58–64.
[32] G.K.P. Dathar, D. Sheppard, K.J. Stevenson, G. Henkelman, Chem. Mater. 23 (2011) 4032–4037.
[33] G.H. Vineyard, J. Phys. Chem. Solids 3 (1957) 121.
[34] K. Kang, D. Morgan, G. Ceder, Phys. Rev. B 79 (2009) 014305.